



HAL
open science

Identification of influence factors in a thermal model of a plasma-assisted chemical vapor deposition process

Sébastien Rouquette, Laurent Autrique, Charles Chaussavoine, Laurent Thomas

► **To cite this version:**

Sébastien Rouquette, Laurent Autrique, Charles Chaussavoine, Laurent Thomas. Identification of influence factors in a thermal model of a plasma-assisted chemical vapor deposition process. *Inverse Problems in Science and Engineering*, 2007, 15 (5), pp.489-515. 10.1080/17415970600838764. hal-04538946

HAL Id: hal-04538946

<https://hal.science/hal-04538946>

Submitted on 15 Apr 2024

HAL is a multi-disciplinary open access archive for the deposit and dissemination of scientific research documents, whether they are published or not. The documents may come from teaching and research institutions in France or abroad, or from public or private research centers.

L'archive ouverte pluridisciplinaire **HAL**, est destinée au dépôt et à la diffusion de documents scientifiques de niveau recherche, publiés ou non, émanant des établissements d'enseignement et de recherche français ou étrangers, des laboratoires publics ou privés.



Distributed under a Creative Commons Attribution - NonCommercial 4.0 International License

Identification of influence factors in a thermal model of a plasma-assisted chemical vapor deposition process

SÉBASTIEN ROUQUETTE*[†], LAURENT AUTRIQUE[‡],
CHARLES CHAUSSAVOINE[†] and LAURENT THOMAS[†]

[†]Institut des Matériaux et Procédés, Tecnosud,
Rambla de la thermodynamique, 66100 Perpignan, France

[‡]Groupe Expertise Hauts Flux (DGA), BP 59,
66121 Font Romeu cedex, France

(Received 6 May 2004; in final form 10 May 2006)

This study is focused on several stages of an identification methodology and consists of selection of the parameters of influence and their identification considering state observations. A partial differential equations system describing the temperature evolution in a plasma-assisted chemical vapor deposition process is investigated. A preliminary study based upon the numerical design of experimental method leads to determination of the parameters which have to be carefully estimated since their uncertainties sharply reduce the adequacy of the model. Then, a sensitivity analysis is performed and the sensitivity problem derived from the direct problem is solved. Optimal observation strategy is briefly discussed in order to obtain state observations for the unknown parameters identification, and a conjugate gradient method is implemented for the resolution of the ill-posed inverse problem.

Keywords: Inverse problem; Numerical design of experiments; Partial differential equations; Sensitivity analysis; Thin film elaboration

1. Introduction

For many industrial processes, the determination of a predictive simulation tool is a helpful step that can avoid unpredictable damage, leads to optimal control procedures, and can then ensure safety processes or economical benefits. In such a way, it is crucial to verify the adequacy of the model and to determine the conditions for which the model is valid. Once the model structure is determined, the set of parameters has to be carefully considered. Parameters' uncertainties and the effect of these uncertainties on the simulation results have to be investigated. Then, for situations where parameters' uncertainties sharply reduce the efficiency of the predictive simulation tool, an identification procedure has to be carried out. This study presents a technique for the estimation of the effect of parameters' uncertainties on numerical results given

*Corresponding author. Email: rouquett@univ-perp.fr

by model simulation. This technique is applied for a thermal situation where the evolution of the temperature (which is the state of the process) is described by a set of nonlinear partial differential equations $\{S_{\text{dir}}\}$. In order to estimate the effect of parameters uncertainties, it is essential to achieve a sensitivity analysis (for informations about sensitivity analysis and experimental design, see [1]). While the evolution of the process state is obtained by considering the simulation of $\{S_{\text{dir}}\}$ (and solving a direct problem), the sensitivity analysis is achieved by computing the sensitivity functions which are solution of the sensitivity problem derived from $\{S_{\text{dir}}\}$. It is usual to reduce the number of uncertain parameters in order to simplify the sensitivity analysis. The choice of the non-studied parameters can be based upon *a priori* knowledge, experimental results, etc. The technique, presented in this study, takes into account the possible uncertainty of all the parameters and does not need a reduction of the set of studied parameters. This technique is based upon the methodology derived from design of experiments (DOE). Usually, a DOE is a set of experimental runs that are chosen in order to estimate the effect of a factor on a response. At the beginning of the twentieth century, experimental investigations methods were developed for agricultural studies (in collaboration with statisticians such as Fisher, for example). These methods were very useful since biological phenomena were quite complex and often considered as black boxes. After the Second World War, factorial designs were used for chemical engineering and the analysis of surface responses was performed in order to identify and fit an appropriate response surface model from experimental data [2]. Then, optimization of processes and quality engineering were investigated (see, for example [3]). In early studies, classical DOE did not make use of model, but in [4] and [5] a DOE method is implemented in a numerical situation. Based upon a model describing the relation between a desired property and some process parameters, optimization is investigated. A set of numerical runs is analyzed and optimal predictions are proposed. The essence of the solution mapping technique presented in [6] is approximation of responses by simple algebraic expressions. The approximating functions are obtained by means of a relatively small number of computer simulations, referred to as computer experiments. They are performed at preselected combinations of the model parameters' values, and the entire set of these combinations is called a design of computer experiments. Computer experiments are arranged in a special order, called factorial design, composed with the objective of minimizing the number of computer experiments to be performed to gain the information required. In [7], a technique for screening, which is the process of searching for the few really important factors among the many great potentially important factors that affect a system's performance, is proposed. In practice, experiments with simulated systems often do involve many factors (for example, >300). The technique is called sequential bifurcation and uses two basic assumptions: the simulation model can be approximated by a low order polynomial approximation (metamodel), and the signs of the main effects are known. A methodology for fitting and validating metamodels in simulation is presented in [8], and it covers four types of goal: understanding, prediction, optimization, and validation. Several metamodel types, including linear regression, neural nets and polynomial metamodels are studied. In [9], sensitivity analysis is used for behaviorally characterizing software process simulators. These characterizations are applied in discussions of improving modeling and of selecting a model, either for unaltered use or for enhancement. Design and analysis of numerical experiments are considered in [10], in order to compare four canopy reflectance models.

In the following, the use of design of numerical experiments is presented in order to study the relative effects of uncertainties of input parameters for a thermal modeling of a plasma-assisted chemical vapor deposition (CVD) process. CVD techniques are developed since the early 1980s in many high technological domains such as microelectronic, optic or aeronautic. In order to obtain ceramic coatings, a microwave PACVD reactor has been developed in the IMP CNRS Institute in Perpignan (France). In previous studies (considering similar technologies), it has been shown that the temperature of the substrate (where the growth of the film occurs) is one of the most important parameter for the elaboration process [11,12]. In that way, it is fundamental to get values as close as possible for the real temperature of plasma-treated substrates in order to:

- collect environmental data for future coating growth simulation,
- establish experimental conditions leading to reproducible deposit temperature,
- investigate technological transfer into industrial scaled reactors.

Thus, thermal model can provide an efficient predictive tool and can lead to the determination of optimal control, diagnosis or supervision procedures in order to control the temperature evolution of the substrate.

This article is organized as follows. The microwave PACVD reactor is briefly presented in the following section. Then, the model describing the temperature evolution is given. A classical system of nonlinear partial differential equation and boundary conditions is considered. Thermophysical characteristics of the materials are given and a direct problem is solved by a finite-element method. Several numerical results are shown. Then, the model is validated and the effect of the parameters uncertainty is investigated. The first method which is exposed is based on a numerical DOE and establishes the model parameters which can be considered as well known. In the second method, by solving sensitivity equations, sensitivity functions are estimated for the parameters for which the uncertainties crucially affect the numerical simulation. In the last section, identification of two parameters is performed considering temperature measurements.

2. Description of the PACVD process

Surface thermal treatments of materials offer an extended field of industrial applications, including the aeronautic, power generation, and engine manufacturing industries. Due to their unique properties such as hardness, or a low-friction coefficient, amorphous silicon carbide films are attractive for mechanical applications [13]. For classical thermal CVD processes, the film is obtained by bringing, in the neighborhood of the substrate surface, a gaseous material for which deposition is ensured by chemical reactions due to high temperature (>1200 K). For PACVD techniques, energy required for the activation of the chemical reaction, is generally provided by a glow discharge sustained by an electrical field, [14]. Moreover, as such techniques use plasmas which are not in thermodynamical equilibrium, deposition can be performed in medium temperature range (300 K \leftrightarrow 1100 K) [15]. This is one of the major interests of such techniques which offer a large choice of substrate materials (plastics to ceramics) and gaseous precursors. Such a technique is developed in the IMP CNRS Institute in Perpignan (France) for the elaboration

of amorphous silicon carbide films for tribological applications. In the experimental reactor studied here [16], a fused silica tube (0.1 m internal diameter) crosses a microwave cavity connected to a 2.45-GHz 1600 W generator through a rectangular surfaguide (figure 1).

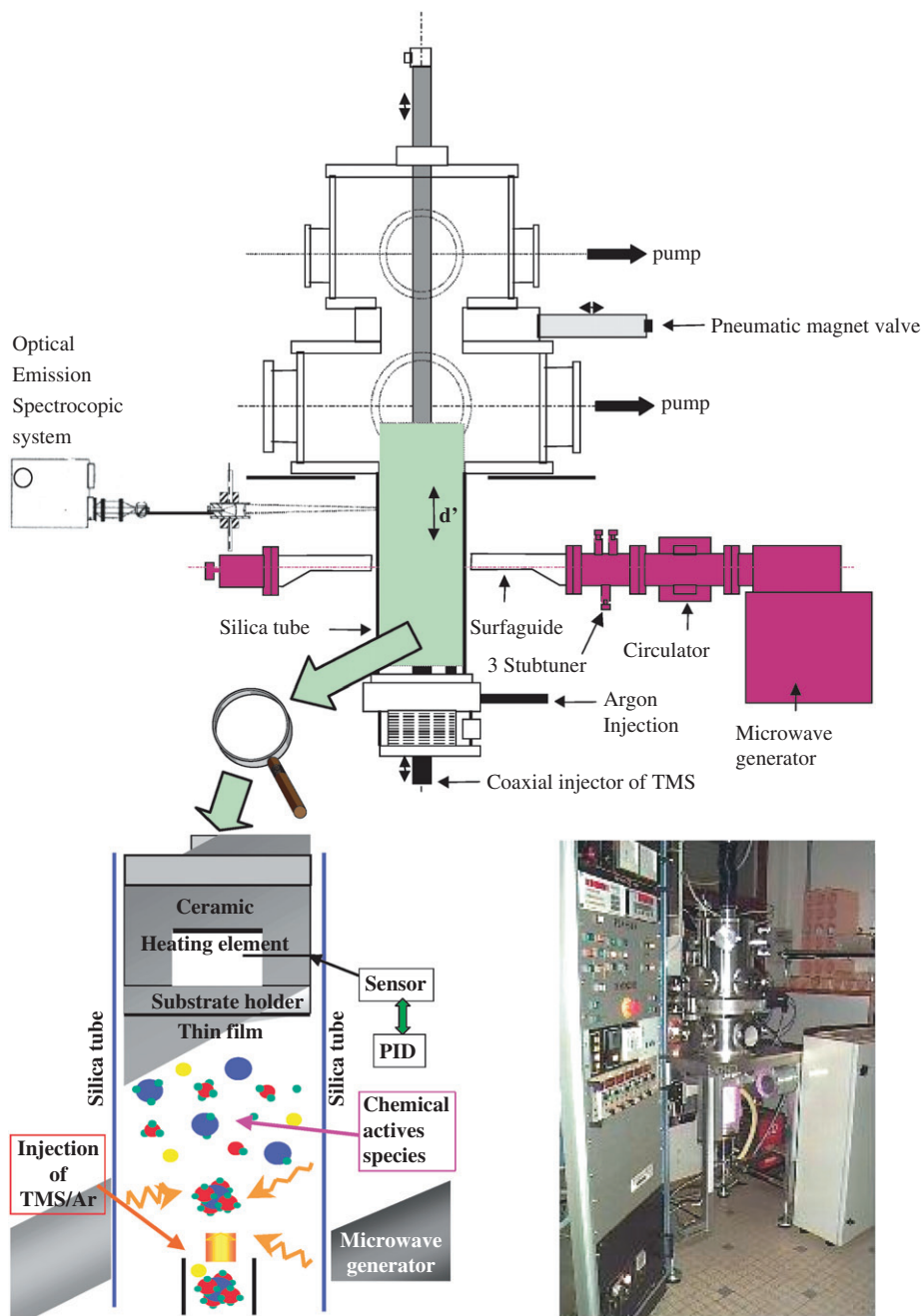


Figure 1. Experimental set-up.

Argon sustains the plasma into which Tetra Methyl Silane (TMS) is fed using a coaxial stainless tube. In the upper part of the reactor, the SiO_2 tube is fitted to a larger steel chamber (0.25 m internal diameter and 0.16 m in height) connected to the pumps (ensuring low working pressures). Films can be grown on silicon or steel substrates set on a movable holder that enables us to control the distance to the precursor inlet d' . The hidden backside of the substrate is heated by a circular thermal source (connected to a PID controller) set in a ceramic support. For technological reasons, the temperature measurements cannot be obtained on the substrate surface. This is an important limitation of the PID efficiency. In this process, Argon(10%) TMS is used as the gas mixture at a total pressure of about 13 Pa and flows at a mean speed close to 2 m s^{-1} when the plasma is off. In order to describe the temperature evolution of the substrate, a 3D modeling of the evolution of the substrate temperature during the process is proposed in the following section.

3. A thermal modeling of the PACVD process

In this study, we are mainly interested in the thermal behavior of the substrate surface (where the growth of the film will occur) before the plasma ignition. In that preliminary heating, the relevant domain is composed of the heating element (PID controlled), the ceramic (support of the heating element), and the substrate holder. The corresponding system is presented in figure 2.

Several substrate shapes can be used in this reactor to avoid an axis-symmetric assumption and a two-dimensional simplification of the geometry. Let us denote by $x = (x_1, x_2, x_3) \in (\bigcup_{i=1,2} \Omega_i) \subset \mathbb{R}^3$, the space variable ($x_3=0$ corresponds to the deposition surface), where Ω_1 corresponds to the substrate holder and Ω_2 corresponds to the substrate. The surface of $\Omega = (\bigcup_{i=1,2} \Omega_i)$ is denoted by $\Gamma = \bigcup_{i=1}^5 \Gamma_i$. The geometry of the studied domain is presented in figure 3:

- Ω_1 corresponds to the substrate holder on the left side of the photograph and the symmetry of the domain leads to the quadrant (radius $3.45 \times 10^{-2} \text{ m}$, height $5 \times 10^{-3} \text{ m}$) with a hole corresponding to Ω_2 ,

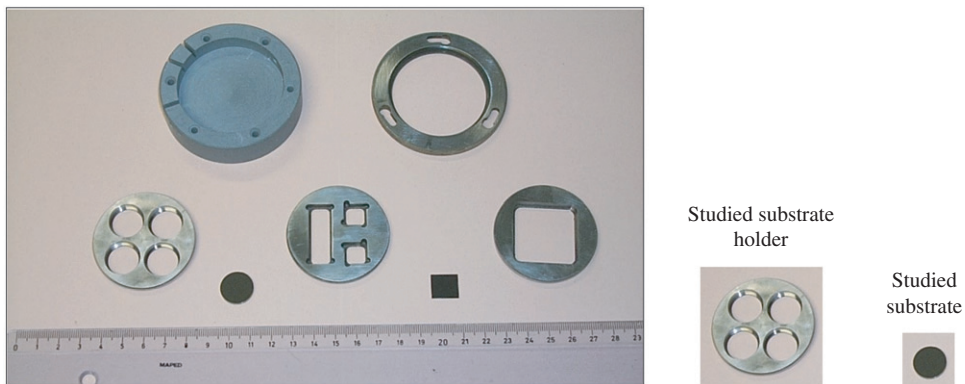


Figure 2. Substrate holder and substrate.

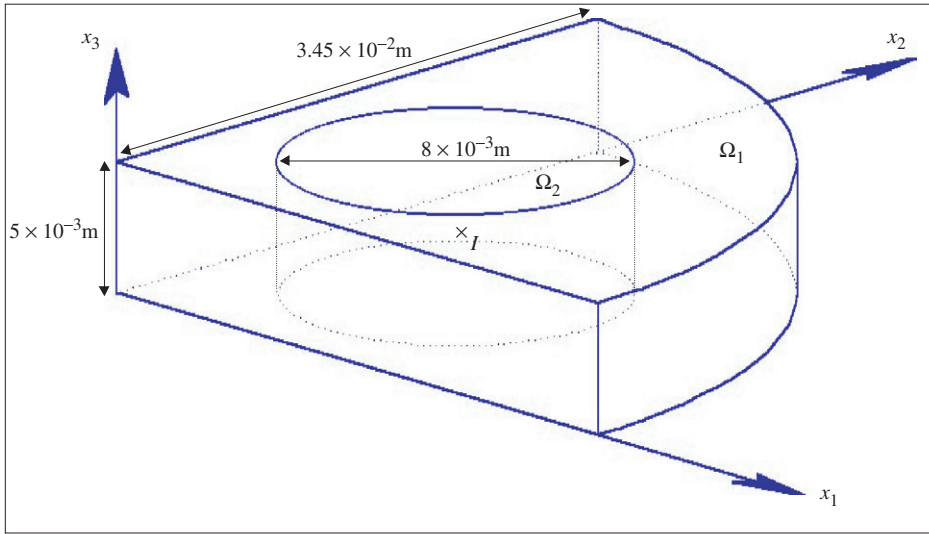


Figure 3. Studied geometry.

- Ω_2 corresponds to a cylindrical substrate (radius 8×10^{-3} m, height 5×10^{-3} m), center: $I(9.44 \times 10^{-3}, 9.44 \times 10^{-3}, 2.5 \times 10^{-3})$.

Let us consider the following notations:

- $t \in T = [0, t_f]$ is the time variable.
- $\theta(x, t)$ is the temperature and the initial temperature is uniform: $\theta_0 = 288$ K.
- Physical and thermal characteristics of the considered steel are denoted by ρ (the mass density), $c(\theta)$ (the specific heat), ε (the emissivity), and $\lambda(\theta)$ (the thermal conductivity).

The thermal evolution of the material during the process is described by the following equations:

- (1) State equations: $\forall (x, t) \in \Omega \times T$

$$\rho c(\theta) \frac{\partial \theta}{\partial t} - \text{div}(\lambda(\theta) \overrightarrow{\text{grad}}(\theta)) = 0. \tag{1}$$

- (2) Initial condition: $\forall x \in \Omega$

$$\theta(x, 0) = \theta_0. \tag{2}$$

- (3) Heat exchange conditions (figure 4):

(a) On the upper face of Ω :

- (i) $\Gamma_1 = \{x \text{ such as } x_3 = 5 \times 10^{-3}\} \cap \{x \text{ such as } (x_1^2 + x_2^2)^{1/2} > 2.67 \times 10^{-2}\}$ corresponds to the surface in contact with the ceramic and $\forall (x, t) \in \Gamma_1 \times T$:

$$-\lambda(\theta) \frac{\partial \theta}{\partial n} = \phi_{c \leftrightarrow c} \tag{3}$$

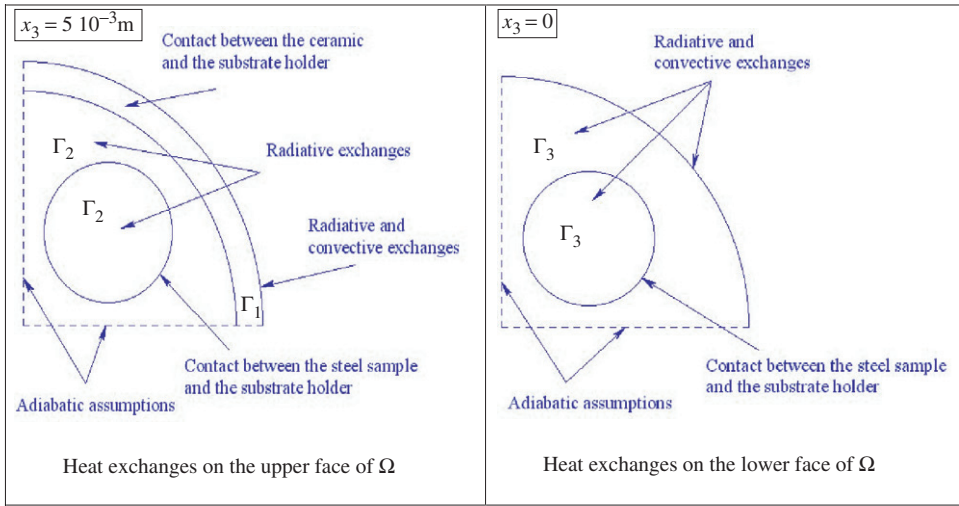


Figure 4. Description of the heat exchanges.

where \vec{n} is the normal vector exterior to the surface and $\phi_{c \leftrightarrow c}$ corresponds to the heat losses between the ceramic and the substrate holder on Γ_1 .

- (ii) $\Gamma_2 = \{x \text{ such as } x_3 = 5 \times 10^{-3}\} \cap \{x \text{ such as } (x_1^2 + x_2^2)^{1/2} \leq 2.67 \times 10^{-2}\}$ corresponds to the surface in front of the heating element and radiative exchanges are considered: $\forall (x, t) \in \Gamma_2 \times T$

$$-\lambda(\theta) \frac{\partial \theta}{\partial \vec{n}} = \varepsilon \sigma (\theta^4 - \theta_h^4(t)) \quad (4)$$

where σ is the Stefan constant and $\theta_h(t)$ is the temperature of the heating element.

- (b) On the lower face and on the lateral circular face of Ω , ($\Gamma_3 = \{x \text{ such as } x_3 = 0\} \cup \{x \text{ such as } (x_1^2 + x_2^2)^{1/2} = 3.45 \times 10^{-2}\}$) convective and radiative exchanges are considered: $\forall (x, t) \in \Gamma_3 \times T$

$$-\lambda(\theta) \frac{\partial \theta}{\partial \vec{n}} = h(\theta)(\theta - \theta_e) + \varepsilon \sigma (\theta^4 - \theta_e^4) \quad (5)$$

where $h(\theta)$ is the convective exchange coefficient on boundary Γ_3 and $\theta_e = 288 \text{ K}$ is the external temperature.

- (c) On the two plane faces ($\Gamma_4 = \{x \text{ such as } x_1 = 0\} \cup \{x \text{ such as } x_2 = 0\}$), due to the symmetry of the domain, one considers: $\forall (x, t) \in \Gamma_4 \times T$

$$-\lambda(\theta) \frac{\partial \theta}{\partial \vec{n}} = 0 \quad (6)$$

- (d) On the boundary Γ_5 between Ω_1 (the substrate holder) and Ω_2 (the cylindrical substrate) a thermal resistance can be considered: $\forall (x, t) \in \Gamma_5 \times T$

$$-\lambda(\theta) \frac{\partial \theta}{\partial \vec{n}} = \frac{1}{R_{1 \rightarrow 2}} \delta_{1 \rightarrow 2}(\theta) \quad (7)$$

where $R_{1 \rightarrow 2}$ is the thermal resistance between Ω_1 and Ω_2 and $\delta_{1 \rightarrow 2}(\theta) = \theta_1(x, t) - \theta_2(x, t)$ is the temperature gap between the two domains (θ_1 (resp. θ_2) is the temperature in Ω_1 (resp. Ω_2)).

According to the previous notations, direct problem can be formulated as follows:

Problem P_{dir} : find the temperature $\theta(x, t)$ solution of the nonlinear partial differential equations system:

$$\{S_{\text{dir}}\} \begin{cases} \text{state equations} & (1) \\ \text{initial condition} & (2) \\ \text{boundary conditions} & (3)(4)(5)(6)(7) \end{cases}$$

Numerical resolution of problem P_{dir} which is standard (the transient conduction equation is solved for the previous specific boundary conditions) is exposed in the following section.

4. Numerical simulation

Except for well-known problems (involving specific nonlinearities and boundary conditions), existence and uniqueness of the solution of problem P_{dir} cannot be stated. Nevertheless, numerical methods such as finite-element method can lead to a numerical determination of state $\theta(x, t)$. Thermophysical properties of the materials are given in table 1. The heat exchanges are simulated according to the following values:

- The heating temperature is: $\theta_h(t) = 1000 \text{ K}$.
- The convective exchange coefficient is quite difficult to estimate. Considering natural convection conditions, the following expression is proposed: $h(\theta) = 0.5(\theta - \theta_c)^{1/3} \text{ W m}^{-2} \text{ K}^{-1}$.
- The Stefan constant is: $5.67 \times 10^{-8} \text{ W m}^{-2} \text{ K}^{-4}$.
- The thermal resistance is about: $R_{1 \rightarrow 2} = 2 \times 10^{-2} \text{ m}^2 \text{ K W}^{-1}$.
- The heat losses between ceramic and substrate holder are estimated from experimental observations: at $t = 0$, $\phi_{c \leftrightarrow c} = 0 \text{ W m}^{-2}$ while for steady state measurements, $\phi_{c \leftrightarrow c} \approx 3000 \text{ W m}^{-2}$. Then, the following evolution is considered: $\phi_{c \leftrightarrow c} = 5(\theta - \theta_0)$.

The time interval is $T = [0; t_f]$ where $t_f = 7200 \text{ s}$; thermal equilibrium is expected by experimentalists after 1800 s. Problem P_{dir} is solved by a finite-element method in space (space step is about 10^{-3} m) and finite difference in time (time step is 5 s).

Table 1. Thermophysical characteristics.

Mass density (kg m^{-3})	Specific heat ($\text{J kg}^{-1} \text{K}^{-1}$)	Thermal conductivity ($\text{W m}^{-1} \text{K}^{-1}$)	Emissivity
$\rho = 7837$	$c(\theta) = \begin{cases} 443.6 + 0.14\theta & \text{if } \theta < 583.3 \\ 391.1 + 0.23\theta & \text{if } 583.3 \leq \theta < 773.3 \\ 275.1 + 0.38\theta & \text{if } \theta > 773.3 \end{cases}$	$\lambda(\theta) = 0.0143\theta + 10.9$	$\varepsilon = 0.2$

Temperature evolutions are shown for points A, B, and C corresponding, on the surface where the deposit occurs, to substrate holder center, substrate center and substrate holder border (figure 5).

In the following figures, several results are presented:

- Figure 6: Temperature evolution at points A, B, and C.
- Figure 7: Temperature spatial distribution at $t_f = 7200$ s on the lower surface (where the deposit occurs).
- Figure 8: Temperature spatial distribution at $t_f = 7200$ s on the upper surface (in front of the heating element).

In figure 6, temperature of the substrate is higher than substrate holder temperature. After about 33 min, 95% of the thermal equilibrium is obtained.

In figure 7, at the end of the simulation, temperature of the lower face of the substrate holder is almost uniform ($640 < \theta < 660$), and temperature of the lower face of the substrate is considered as uniform ($714.7 < \theta < 715.7$).

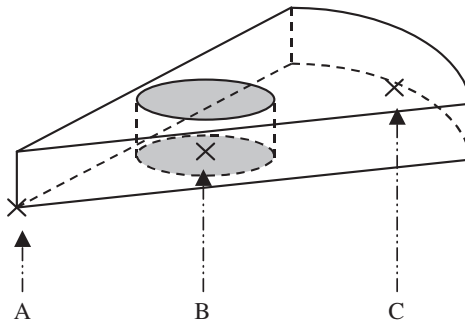


Figure 5. Positions A, B and C.

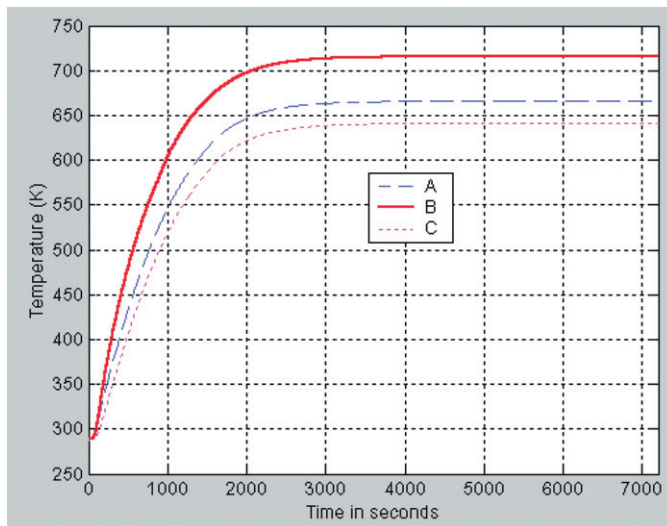


Figure 6. Temperature evolution at positions A, B, and C.

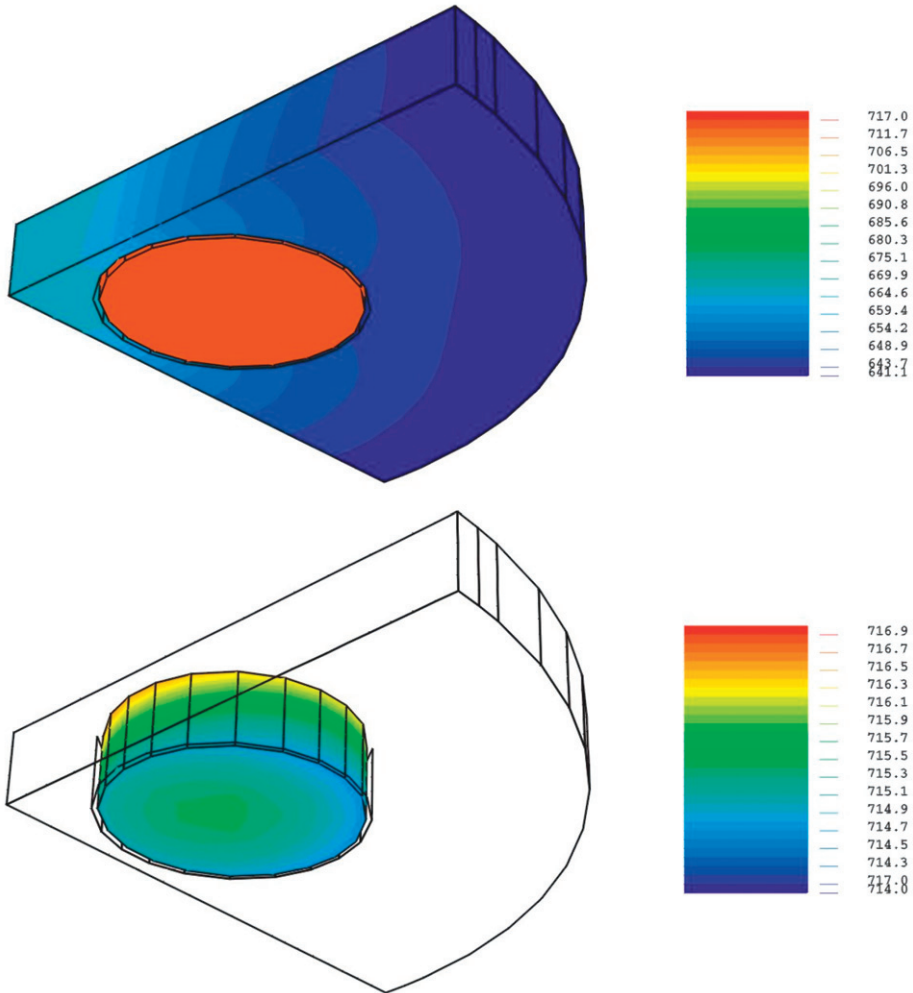


Figure 7. Temperature spatial distribution at $t_f = 7200$ s on the lower surface.

In figure 8, at the end of the simulation, temperature of the upper face of the substrate holder is almost uniform ($640 < \theta < 660$), and temperature of the upper face of the substrate is considered as uniform ($716 < \theta < 717$). Previous numerical results correspond to experimental observations: deposit process has to be started after 30 min of a heating cycle and temperature of the substrate is uniform. In order to estimate which parameters' uncertainties sharply reduce numerical results accuracy and have to be identified (according to inverse method [17]), a numerical DOE approach is proposed in the following section.

5. Numerical investigations for finding the factors of influence

Effect of parameters' uncertainty is investigated using a DOE procedure see [18,19], for example. Two-level factorial design is particularly useful in the early stages of

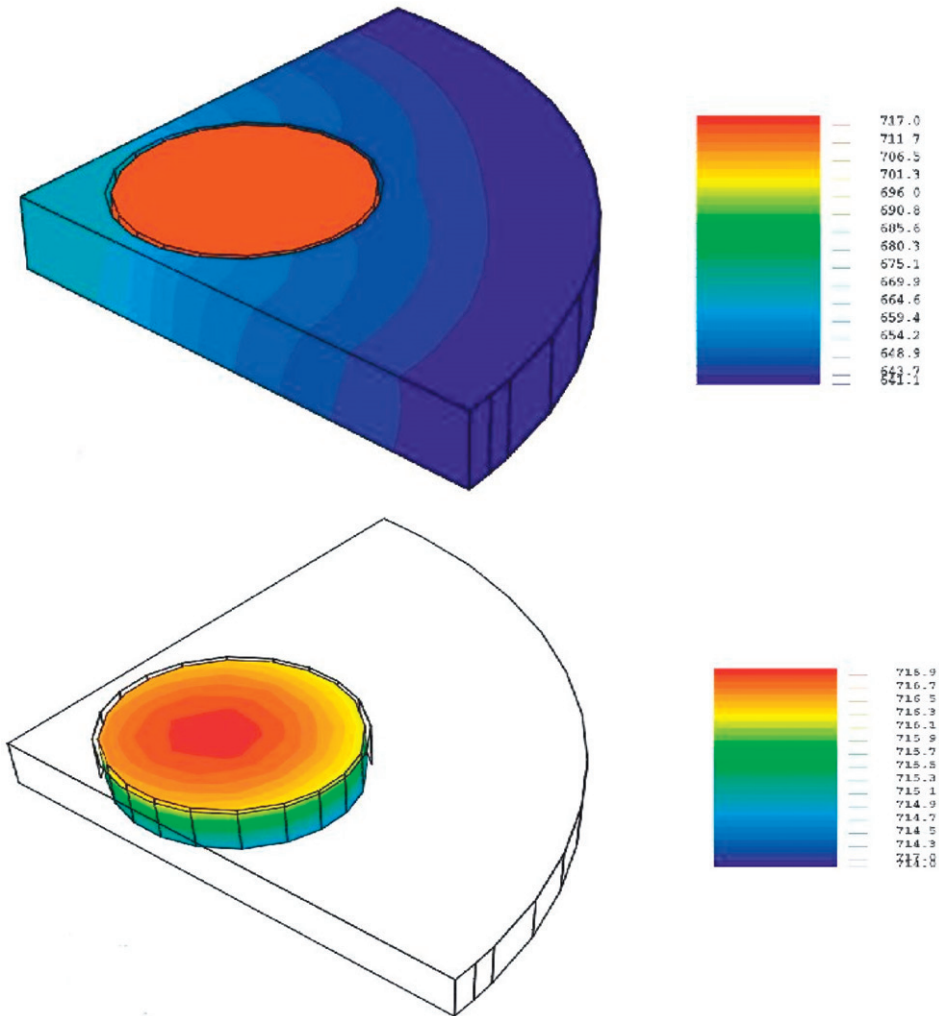


Figure 8. Temperature spatial distribution at $t_r = 7200$ s on the upper surface.

experimental work, when there are likely many factors to be investigated. The aim of this approach is to identify the critical model factors and to provide information about which factors should be more carefully controlled to prevent high numerical variation of the model responses. Such a strategy is sometimes called screening or characterization experiments. DOE method is usually implemented in experimental situations where a model is not available. In the specific framework of this communication, a physical model is already established. This work is focused on the numerical sensitivity of the model. DOE strategy is applied to numerical results (obtained from several simulations based on a finite-element method in 3D geometry). Each run leads to a simulation and numerical results are obtained without experimental unknown disturbances (noises). Thus, statistical analysis (for example, significance tests determination of confidence intervals) are meaningless. However, in [4], the DOE approach is implemented in order to investigate the effect of unknown factors for numerical simulations. Several physical

Table 2. Levels of parameters.

	1	2	3	4	5	6	7
Factors	$\rho c(\theta)$	$\lambda(\theta)$	$h(\theta)$	ε	$\phi_{c \leftrightarrow c}$	$R_{1 \rightarrow 2}$	$\theta_h(t)$
Level (-)	-5%	-5%	-50%	-20%	-50%	-50%	-5%
Level (+)	+5%	+	+50%	+20%	+50%	+0%	+5%

Table 3. The preliminary 2^{7-4} fractional factorial design.

Run	1	2	3	4 = 123	5 = 12	6 = 23	7 = 13
1	-	-	-	-	+	+	+
2	+	-	-	+	-	+	-
3	-	+	-	+	-	-	+
4	+	+	-	-	+	-	-
5	-	-	+	+	+	-	-
6	+	-	+	-	-	-	+
7	-	+	+	-	-	+	-
8	+	+	+	+	+	+	+

inputs in the nonlinear partial differential equation or in the boundary conditions are considered:

- Thermophysical parameters known with a given indeterminacy: $\rho c(\theta)$, $\lambda(\theta)$.
- Thermophysical and experimental parameters which are not well known: convective exchange coefficient $h(\theta)$, emissivity ε , $\phi_{c \leftrightarrow c}$ the heat losses between the ceramic and the substrate holder and the thermal resistance $R_{1 \rightarrow 2}$.
- Experimental conditions: heating element temperature $\theta_h(r)$.

However, it is obvious that these factors have to be taken into account in different ways. For example, based on the experimentation and the process knowledge, it seems that factor $\theta_h(r)$ is crucial but can be measured or controlled. However, influence of factors $h(\theta)$, ε , $\phi_{c \leftrightarrow c}$, and $R_{1 \rightarrow 2}$ is quite difficult to estimate.

Remark Initial temperature θ_0 and external temperature θ_e are not considered in the numerical DOE study since θ_0 is easily measured with a great precision and the influence of θ_e is connected to factors h and ε .

Numerical simulation, obtained from the parameters' values defined in section 4, is considered as the reference for the temperature evolution $\theta_{ref}(x, t)$ in the domain Ω (figures 5–7). An appropriate scaling for each of the parameters' inaccuracy is chosen. The range is defined between two levels, from the parameters' values given in section 4 (these levels are arbitrarily called low (-) and high (+)) (table 2).

The effect of a factor is defined to be the change in response produced by a change in the level of the factor. In this study, it corresponds to the effect on the simulation results of a scanning of the confidence interval for each physical parameter (model input). This is frequently called a main effect because it refers to the primary factors of interest in the experiment. A complete factorial design, where the whole configuration is investigated, requires 2^7 observations (simulations). However, correct analysis can be performed with few simulations by introducing a 2^{7-4} fractional factorial design [19]. In this communication, it is implemented by choosing 4 design generators, which are defined

Table 4. Results of the preliminary 2^{7-4} fractional factorial design.

Run	θ_A	θ_B	θ_C	δ_1	δ_2	$t_{95\%}$
1	709.9	746.1	683.3	1.02	2.46	2055
2	678.1	706.2	655.9	0.84	2.31	2005
3	741.0	823.6	715.7	0.47	2.30	1235
4	615.2	689.3	597.4	0.43	1.36	2825
5	601.1	684.1	574.8	0.58	2.25	1605
6	661.7	743.0	637.9	0.53	2.19	2055
7	594.8	619.4	577.7	0.66	1.75	2575
8	693.5	740.0	659.9	1.17	3.28	1485

according to the box notation: $I = 1234 = 125 = 236 = 137$. These relations are the key to the confounding pattern [20]. In table 3, the column of sign for 123 interaction is used to define the levels of variable 4. Equivalently, in this factorial design 123 and 4 are said to be aliases of each other; 12 and 5 (23 and 6) (13 and 7) are aliases of each other. The design is obtained by associating every available interactions (of initial complete factorial design 2^3) with a variable and is therefore called a saturated design.

This preliminary study leads to the resolution of 8 direct problems corresponding to eight physical parameters' configurations. For example, for numerical run 6, problem P_{dir} is solved with the following parameters' values:

$$(1) \rho_c(\theta) = 1.05[7837] \left[\begin{cases} 443.6 + 0.14\theta & \text{if } \theta < 583.3 \\ 391.1 + 0.23\theta & \text{if } 583.3 \leq \theta < 773.3 \\ 275.1 + 0.38\theta & \text{if } \theta > 773.3 \end{cases} \right]$$

$$(2) \lambda(\theta) = 0.95[0.0143\theta + 10.9] \qquad (5) \phi_{c \leftrightarrow c} = 0.5[2000]$$

$$(3) h(\theta) = 1.05[0.5(\theta - \theta_c)^{1/3}] \qquad (6) R_{1 \rightarrow 2} = 0.5[2 \times 10^{-2}]$$

$$(4) \varepsilon = 0.8[0.2] \qquad (7) \theta_h(t) = 1.05[1000]$$

In order to determine the effect of the model parameters on simulation results, several responses are considered:

- $\theta_A, \theta_B, \theta_C$ (K): final temperature at points A, B, and C,
- δ_1 (K): maximum temperature difference on the substrate lower face,
- δ_2 (K): maximum temperature difference between the upper and the lower face of the substrate,
- $t_{95\%}$ (s): the instant for which 95% of the final temperature at point B is obtained.

One can notice that for experimentalists, $\theta_B, \delta_1,$ and δ_2 are essential to ensure the reproducibility of the deposit, and that $t_{95\%}$ is an important parameter for the control of the reactor since deposit process begins after temperature is stabilized. Results corresponding to the 8 simulations defined in table 3 are given in table 4.

The alias structure of this design is easily determined and main effects are aliased to two-factors interactions (and to more interactions): **1** + 25 + 37 + 46; **2** + 15 + 36 + 47; **3** + 17 + 26 + 45; **4** + 16 + 27 + 35; **5** + 12 + 34 + 67; **6** + 14 + 23 + 57; **7** + 13 + 24 + 56. Considering tables 3 and 4, effect of each parameter uncertainty can be estimated. Effects are given in table 5. For example, for column corresponding to factor 1 in table 3, simulations 1, 3, 5, and 7 are performed according to level (−) and simulations 2, 4, 6, and 8 are performed according to level (+). Then, comparisons between

Table 5. Effects obtained from the preliminary 2^{7-4} fractional factorial design.

Factor	θ_A (K)	θ_B (K)	θ_C (K)	δ_1 (K)	δ_2 (K)	$t_{95\%}$ (s)
$\rho c(\theta)$ (1) +25 + 37 + 46	0.4	1.3	-0.1	0.1	0.1	225.0
$\lambda(\theta)$ (2) +15 + 36 + 47	-1.6	-1.8	-0.3	-0.1	-0.1	100.0
$h(\theta)$ (3) +17 + 26 + 45	-48.3	-44.7	-50.5	0.0	0.3	-100.0
ε (4) +16 + 27 + 35	33.0	39.0	27.5	0.1	0.6	-795.0
$\phi_{c \leftrightarrow c}$ (5) +12 + 34 + 67	-14.0	-8.2	-18.0	0.2	0.2	25.0
$R_{1 \rightarrow 2}$ (6) +14 + 23 + 57	14.3	-32.1	12.8	0.4	0.4	100.0
$\theta_h(t)$ (7) +13 + 24 + 56	79.2	88.4	72.8	0.2	0.6	-545.0

Table 6. The complementary 2^{7-4} fractional factorial design.

Run	(1)	(2)	(3)	(4 = 123)	(5 = -12)	(6 = -23)	(7 = -13)
9	-	-	-	-	-	-	-
10	+	-	-	+	+	-	+
11	-	+	-	+	+	+	-
12	+	+	-	-	-	+	+
13	-	-	+	+	-	+	+
14	+	-	+	-	+	+	-
15	-	+	+	+	+	-	+
16	+	+	+	-	-	-	-

numerical results shown in table 4, lead to the following analysis: if $(\rho c(\theta))$ is varying between $\pm 5\%$ then the average effect on estimated temperature θ_A is:

$$\frac{(678.1 + 615.2 + 661.7 + 693.5)}{4} - \frac{(709.9 + 741.0 + 601.1 + 594.8)}{4} \approx 0.42$$

Let the interactions effects assumed to be equal to zero, then this results seem to confirm that the indeterminacy for the physical characteristics $(\rho c(\theta), \lambda(\theta))$ is not very significant. Moreover, inaccuracies on $\phi_{c \leftrightarrow c}$ (the heat losses between the ceramic and the substrate holder) and on $R_{1 \rightarrow 2}$ (the thermal resistance) do not affect the chosen output. Convective exchange coefficient $h(\theta)$ and emissivity ε have to be better determined. The heating temperature $\theta_h(t)$ is very important: for example, an error in the studied range ($\pm 5\%$) seems to lead to an error of 88 K on the simulated temperature of the substrate and to an error of 9 min on $t_{95\%}$. In order to investigate the two-factors interactions effects, a complementary fraction is investigated:

Previous numerical runs are chosen according to the following design generators: $\mathbf{I} = \mathbf{1234} = -\mathbf{125} = -\mathbf{236} = -\mathbf{247}$. Results corresponding to the eight further simulations are shown in table 7; corresponding effects are given in table 8.

Then, comparison between tables 5 and 8 leads to the determination of the main effects and interactions. For example, in table 5 $\rho c(\theta) + 25 + 37 + 46 \approx 0.4$, and in table 8 $\rho c(\theta) - 25 - 37 - 46 \approx -0.6$ then $\rho c(\theta) \approx -0.1$ and $25 + 37 + 46 \approx 0.5$.

Comments:

- $\rho c(\theta)$ and $\lambda(\theta)$ are well known and in the range ($\pm 5\%$), numerical results are accurate enough,
- δ_1 and δ_2 are not affected by errors on the model parameters and the temperature in the substrate can be considered as uniform,

Table 7. Results of the complementary 2^{7-4} fractional factorial design.

Run	θ_A	θ_B	θ_C	δ_1	δ_2	$t_{95\%}$
9	648.4	707.6	632.4	0.39	1.40	2600
10	722.1	816.2	690.4	0.61	2.64	1355
11	655.8	689.9	631.9	0.88	2.22	1830
12	736.0	767.4	715.6	0.74	2.03	2275
13	712.3	752.4	679.5	1.17	3.49	1360
14	572.5	599.8	550.8	0.88	2.09	2765
15	635.3	730.5	610.5	0.55	2.05	1840
16	618.8	692.6	597.6	0.45	1.96	1810

Table 8. Effects obtained from the preliminary 2^{7-4} fractional factorial design.

Factor	θ_A	θ_B	θ_C	δ_1	δ_2	$t_{95\%}$
$\rho_c(\theta)$ (1) -25-37-46	-0.6	-1.1	0.0	-0.1	-0.1	143.8
$\lambda(\theta)$ (2) -15-36-47	-2.4	1.1	0.6	-0.1	-0.3	-81.3
$h(\theta)$ (3) -17-26-45	-55.9	-51.5	-58.0	0.1	0.3	-71.3
ε (4) -16-27-35	29.2	36.5	22.5	0.1	0.7	-781.3
$\phi_{c \leftrightarrow c}$ (5) -12-34-67	-32.5	-20.9	-35.4	0.0	0.0	-63.8
$R_{1 \rightarrow 2}$ (6) -14-23-57	13.0	-34.4	11.7	0.4	0.4	156.3
$\theta_h(t)$ (7) -13-24-56	77.6	94.2	70.8	0.1	0.6	-543.8

- The heating temperature $\theta_h(t)$ is very important: for example, an error in the studied range ($\pm 5\%$) seems to lead to an error of about 10% on the simulated temperature and to an error of about 30% on $t_{95\%}$.
- The convective exchanges $h(\theta)$ has to be known with a better accuracy in order to determine the final temperature: in the range ($\pm 50\%$), an error of 50 K is expected,
- Emissivity of the steel ε has to be carefully determined in order to predict $t_{95\%}$ (corresponding to the beginning of the deposition process): in the range ($\pm 20\%$), an error of 13 min is expected.

In order to establish an accurate predictive model, the temperature of the heating element has to be measured with great precision and convective exchange $h(\theta)$ and emissivity ε have to be identified. In such a way, an inverse problem can be considered: from temperature measurements in Ω a quadratic criterion (describing the error between numerical results and experimental results) is minimized. For this ill-posed problem, a conjugate gradient method can be implemented and leads to the iterative resolution of three well-posed problems: the direct problem in order to estimate the cost function, the adjoint problem in order to determine the cost function gradient and the descent direction and the sensitivity problem in order to calculate the descent depth. Sensitivity equations are exposed in the following section.

6. Sensitivity analysis

In this section, sensitivity equations are written according to the method exposed in [21] for an application. For this method, an initial value of the unknown parameter ($h(\theta)$ or ε) has to be considered. A partial knowledge of the physical signification of these

parameters can be taken into account and thermophysical characteristics given in table 1 can be considered. Let us denote by f the unknown parameter ($f = h(\theta)$ or $f = \varepsilon$). The sensitivity function corresponding to a state variation resulting of a parameter variation ($\mu\delta f$) is defined as: $\delta\theta(x, t; f) = \lim_{\mu \rightarrow 0} \theta(x, t; f + \mu\delta f) - \theta(x, t; f)/\mu$. Differentiating the model equations given in problem P_{dir} , the system satisfied by $\delta\theta(x, t; f)$ reads as follows:

$$\forall (x, t) \in \Omega \times T : \quad \rho c(\theta) \frac{\partial \delta\theta}{\partial t} + \delta\theta \frac{\partial(\rho c(\theta))}{\partial \theta} \frac{\partial \theta}{\partial t} - \text{div} \left(\lambda \overrightarrow{\text{grad}}(\delta\theta) + \delta\theta \frac{\partial \lambda}{\partial \theta} \overrightarrow{\text{grad}}(\theta) \right) = 0 \quad (8)$$

$$\text{at } t = 0 : \quad \forall x \in \Omega \quad \delta\theta = 0 \quad (9)$$

$$\forall (x, t) \in \Gamma_1 \times T \quad -\lambda \frac{\partial \delta\theta}{\partial \bar{n}} - \delta\theta \frac{\partial \lambda}{\partial \theta} \frac{\partial \theta}{\partial \bar{n}} = 0 \quad (10)$$

$$\forall (x, t) \in \Gamma_2 \times T \quad -\lambda \frac{\partial \delta\theta}{\partial \bar{n}} - \delta\theta \frac{\partial \lambda}{\partial \theta} \frac{\partial \theta}{\partial \bar{n}} = \begin{cases} \sigma(\delta\varepsilon(\theta^4 - \theta_h^4) + 4\varepsilon\theta^3\delta\theta) & \text{if } f = \varepsilon \\ 4\varepsilon\sigma\theta^3\delta\theta & \text{if } f = h \end{cases} \quad (11)$$

$$\forall (x, t) \in \Gamma_3 \times T, \quad -\lambda \frac{\partial \delta\theta}{\partial \bar{n}} - \delta\theta \frac{\partial \lambda}{\partial \theta} \frac{\partial \theta}{\partial \bar{n}} = \begin{cases} h\delta\theta + \delta\theta \frac{\partial h}{\partial \theta} (\theta - \theta_e) + \sigma(\delta\varepsilon(\theta^4 - \theta_e^4) + 4\varepsilon\theta^3\delta\theta) & \text{if } f = \varepsilon \\ h\delta\theta + \left(\delta\theta \frac{\partial h}{\partial \theta} + \delta h \right) (\theta - \theta_e) + 4\varepsilon\sigma\theta^3\delta\theta & \text{if } f = h \end{cases} \quad (12)$$

$$\forall (x, t) \in \Gamma_4 \times T \quad -\lambda \frac{\partial \delta\theta}{\partial \bar{n}} - \delta\theta \frac{\partial \lambda}{\partial \theta} \frac{\partial \theta}{\partial \bar{n}} = 0 \quad (13)$$

$$\forall (x, t) \in \Gamma_5 \times T \quad -\lambda \frac{\partial \delta\theta}{\partial \bar{n}} - \delta\theta \frac{\partial \lambda}{\partial \theta} \frac{\partial \theta}{\partial \bar{n}} = \frac{1}{R_{1 \rightarrow 2}} (\delta_{1 \rightarrow 2}(\delta\theta)) \quad (14)$$

According to the previous notations, sensitivity problem can be formulated as:

Problem P_{sens} : find the temperature variation $\delta\theta(x, t)$ solution of the partial differential equations system:

$$\{S_{sens}\} \begin{cases} \text{state equations} & (8) \\ \text{initial condition} & (9) \\ \text{boundary conditions} & (10)(11)(12)(13)(14) \end{cases}$$

Sensitivity problem is solved for a variation: $\delta f = (1/100)f$ and results are given for $f = h(\theta)$ (case 1) and $f = \varepsilon$ (case 2).

- Case 1: $f = h(\theta)$. In the following figures, several results are presented:
 - (i) Figure 9: (1) sensitivity evolution at points A, B, and C.
 - (ii) Figure 10: (1) sensitivity spatial distribution at 3600 s on the lower surface (where the deposit occurs).
 - (iii) Figure 11: (1) sensitivity spatial distribution at 3600 s on the upper face (in front of the heating element).

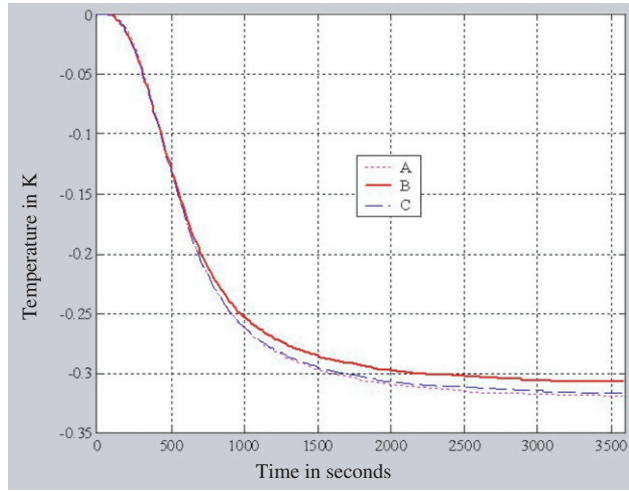


Figure 9. (#1) Sensitivity evolution at positions A, B, and C.

In figure 9, sensitivity to convective exchange coefficient h is more important at the end of the simulation. According to the previous result, sensitivity to convective coefficient h is three times greater in the last 25 min than in the first 7 min. Then, for identification of convective heat exchange coefficient, temperature measurements have to be less taken into account in the early minutes. Moreover, these results can be compared to those obtained by the numerical DOE exposed in section 4. In fact, it has been shown in table 9 that temperature at the end of the simulation is more affected at sensor C by uncertainty on $h(\theta)$ and less affected at sensor B. This comment is also illustrated in figure 9. The effect of the given uncertainty ($\pm 50\%$) is estimated by the numerical DOE equal to -54.2 K for sensor C temperature at 3600 s. Thus, for a variation equal to $+1\%$, this effect should be equal to -0.54 K. In figure 9, the sensitivity function is equal to -0.32 K at 3600 s. This difference is due to the nonlinearity of the direct model and due to the strong hypothesis required to neglect the interactions between more than two factors in the fractional factorial design analysis.

In figures 10 and 11, at the end of the simulation, sensitivity to h is considered as uniform ($-0.179 < \delta\theta < -0.168$), then temperature measurements for identification purpose can be located anywhere in the whole domain.

- Case #2: $f = \varepsilon$. In the following figures, several results are presented:
 - (i) Figure 12: (2) sensitivity evolution at points A, B and C.
 - (ii) Figure 13: (2) sensitivity spatial distribution at 3600 s on the lower face (where the deposit occurs).
 - (iii) Figure 14: (2) sensitivity spatial distribution at 3600 s on the upper face.

In figure 12, sensitivity to emissivity is maximum at $t = 720$ s and:

- (i) for $t \in [175; 935]$ then $\delta\theta_{\max}/2 < \delta\theta < \delta\theta_{\max}$,
- (ii) for $t \in [115; 1490]$ then $\delta\theta_{\max}/4 < \delta\theta < \delta\theta_{\max}$.

Then, for identification of emissivity coefficient, temperature measurements do not have to be taken in the first minutes and for long time observations. The previous

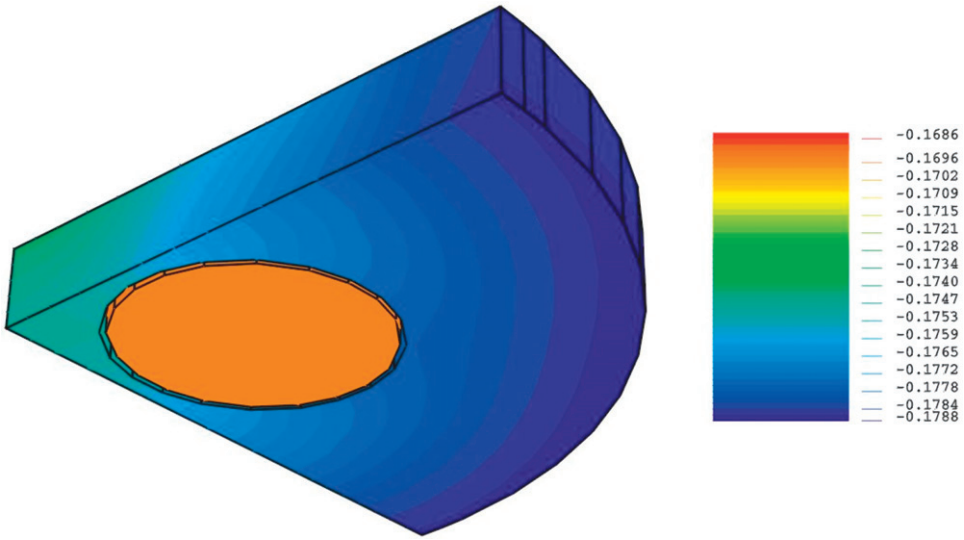


Figure 10. (#1) Sensitivity spatial distribution at $t_f=3600$ s on the lower surface.

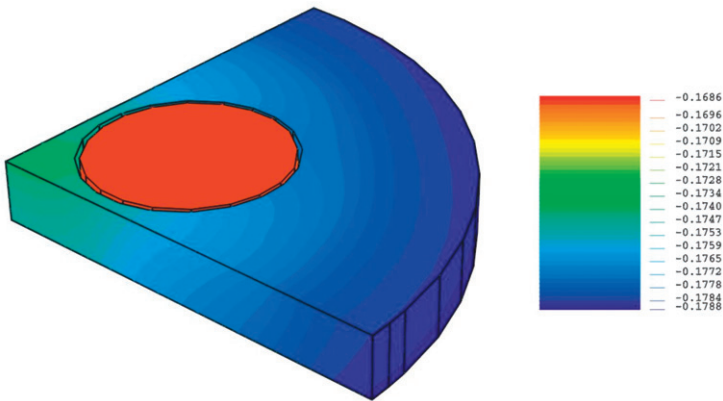


Figure 11. (#1) Sensitivity spatial distribution at $t_f=3600$ s on the upper surface.

numerical DOE (section 4) has been implemented for a given emissivity uncertainty

Table 9. Main effects.

Factor	θ_A	θ_B	θ_C	δ_1	δ_2	$t_{95\%}$
$\rho_c(\theta)$	-0.1	0.1	0.0	0.0	0.0	184.4
$\lambda(\theta)$	-2.0	-0.3	0.2	-0.1	-0.2	9.4
$h(\theta)$	-52.1	-48.1	-54.2	0.1	0.3	-85.6
ε	31.1	37.7	25.0	0.1	0.6	-788.1
$\phi_{c \leftrightarrow c}$	-23.2	-14.5	-26.7	0.1	0.1	-19.4
$R_{1 \rightarrow 2}$	13.7	-33.2	12.2	0.4	0.4	128.1
$\theta_h(t)$	78.4	91.3	71.8	0.1	0.6	-544.4

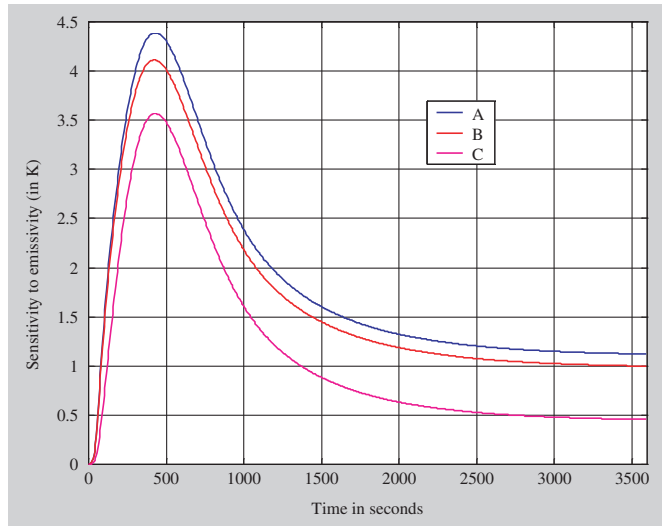


Figure 12. (#2) Sensitivity evolution at positions A, B and C.

(±20%) and the effect on simulated temperature is only estimated at the end of the simulation. Thus, the maximum effect of emissivity uncertainty has not been observed with the numerical DOE method. However, the effect on the stabilization time $t_{95\%}$ is not easily brought to the fore by the resolution of sensitivity equations $\{S_{sens}\}$. Then, both of the approaches are complementary.

In figures 13 and 14, at the end of the simulation, sensitivity to emissivity ε is not uniform ($0.454 < \delta\theta < 1.226$), and at point A (middle of the substrate holder), sensitivity is two times greater than on the substrate holder edge.

Then, for the identification of the convective exchange coefficient and of the emissivity, an inverse problem has to be solved and temperature measurements are required. Optimal sensor location is the heated substrate holder center and on several time samples are considered since sensitivity to emissivity factor is maximum during the first 25 min and sensitivity to convective exchange coefficient is greater in the last 35 min.

7. Parameters' identification

As stated earlier, the knowledge of the emissivity and convective exchange coefficients is crucial for the thermal modeling accuracy. Let us denote by $f = \{\varepsilon(\theta), h(\theta)\}$, the unknown parameters (or functions) which have to be identified. The general formulation of the inverse boundary problem can be written as follows:

Find $f = \{\varepsilon(\theta), h(\theta)\}$ such that the following quadratic criterion is minimum.

$$J(f, \theta) = \frac{1}{2} \int_T \int_{\Omega} \sum_{i=1}^{n_C} (\theta(x_i, t) - \hat{\theta}_{mes}(x_i, t))^2 \delta(x - x_i) dt d\Omega$$

where the $\hat{\theta}_{mes}(x_i, t)$ is the measured temperature at each sensor located at points x_i , $i = 1, n_C$, n_C is the number of sensors, $\theta(x, t)$ is the simulated temperature and $\delta(x)$ is the Dirac function.

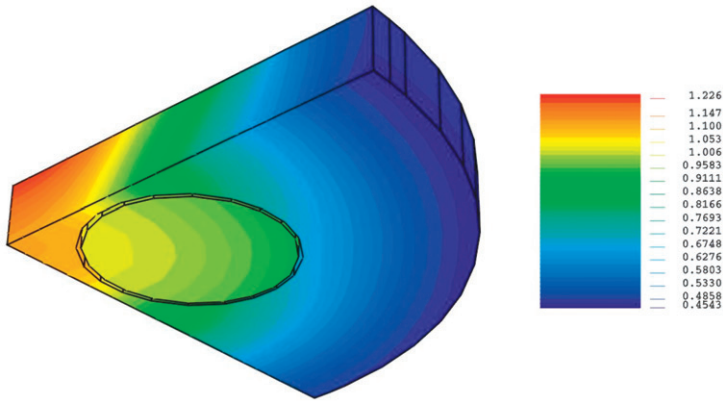


Figure 13. (#2) Sensitivity spatial distribution at $t_f=3600$ s on the lower surface.

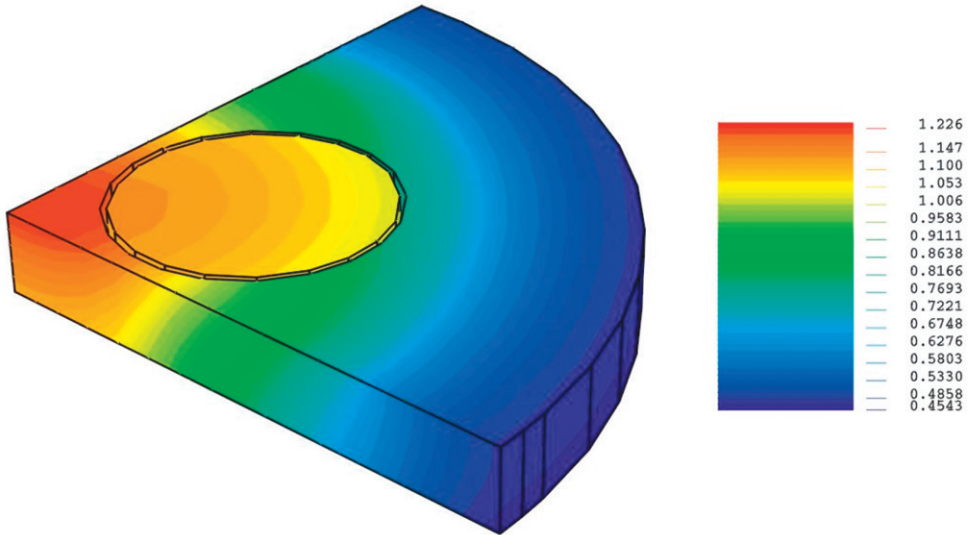


Figure 14. (#2) Sensitivity spatial distribution at $t_f=3600$ s on the upper surface.

7.1. Minimization algorithm

For the resolution of such an ill-posed inverse problem, a regularization method is required and the iterative conjugate gradient method (CGM) proposed in [22] is implemented. At each iteration n of this minimization algorithm, the estimated function f is calculated according to a descent method: $f^{n+1} = f^n + \gamma_n d^n$ where n is the iteration parameter. γ_n is the descent depth and d^n is the descent direction at the iteration n . The main requirements of the CGM are the descent depth and the descent direction. The descent direction d^n (also called conjugate direction) is: $d^n = d^{n-1} + \nabla J(f^n, \theta)$, where $\nabla J(f^n, \theta)$ is the gradient of the cost function to minimize. The descent depth γ_n is

determined such as: $\gamma_n = \arg \min_{\gamma \in \mathbb{R}} (J(\theta, f^n - \gamma d^n))$. In [21], the solution of these equation is formulated as follows:

$$\gamma = \frac{\int_T \int_{\Omega} \sum_{i=1}^{n_c} (\theta(x, t; f) - \hat{\theta}_{\text{mes}}(t))^2 \delta \theta \delta(x - x_i) dt d\Omega}{\int_T \int_{\Omega} \sum_{i=1}^{n_c} \delta \theta^2 \delta(x - x_i) dt d\Omega}$$

For the computation of the descent depth γ , the sensitivity functions $\delta \theta$ (at each sensor and at each instant) are required. The sensitivity equations have been previously defined in section 6. Then, in the following, the adjoint problem is briefly exposed in order to compute the descent direction and the cost function gradient. The gradient is obtained by solving the Lagrange equation associated to the cost function minimization problem:

$$\begin{aligned} \mathcal{L}(\theta, z, \psi) = & \frac{1}{2} \int_t \int_{\Omega} \sum_{i=1}^{n_c} (\theta(x, t; z) - \hat{\theta}_{\text{mes}}(t))^2 \delta(x - x_i) dt d\Omega \\ & + \int_t \int_{\Omega} \left(\rho C(\theta) \frac{\partial \theta}{\partial t} - \nabla(\lambda(\theta) \nabla \theta) \right) \psi dt d\Omega \end{aligned}$$

where ψ is the Lagrangian function. The adjoin equations are verified when $(\partial \mathcal{L} / \partial \theta) \delta \theta = 0$ for a fixed value of ψ . The achievement of the adjoin equations is detailed in [21] and [22] and the following system is considered:

$$S_{ADJ} \left\{ \begin{aligned} & -C(\theta) \frac{\partial \psi}{\partial t} - \lambda(\theta) \Delta \psi = 0 \quad \text{in } \Omega \times T \\ & -\lambda(\theta) \frac{\partial \psi}{\partial \vec{n}_1} = \left[h(\theta) + \frac{\partial h(\theta)}{\partial \theta} (\theta - \theta_{\text{amb}}) + 4\varepsilon(\theta) \sigma \theta^3 + \frac{\partial \varepsilon(\theta)}{\partial \theta} \sigma (\theta^4 - \theta_{\text{amb}}^4) \right] \psi \quad \text{on } \Gamma_1 \times T \\ & -\lambda(\theta) \frac{\partial \psi}{\partial \vec{n}_2} = \left[4\varepsilon(\theta) \sigma \theta^3 + \frac{\partial \varepsilon(\theta)}{\partial \theta} \sigma (\theta^4 - \theta_{\text{hot}}^4) \right] \psi \quad \text{on } \Gamma_2 \times T \\ & -\lambda(\theta) \frac{\partial \psi}{\partial \vec{n}_3} = \left[R(\theta) + \frac{\partial R(\theta)}{\partial \theta} (\theta - \theta_{\text{ceram}}) \right] \psi \quad \text{on } \Gamma_3 \times T \\ & \psi(x, t_f) = 0 \quad \text{in } \Omega \text{ à } t = t_f \end{aligned} \right.$$

Temperature distributions are required for the adjoint problem resolution, then the direct problem has to be solved. Considering $\delta \mathcal{L}(\theta, \psi, f) = \langle \nabla J(\theta, f), \delta f \rangle$,

- the cost function gradient for $f = \varepsilon$ is:

$$\nabla J_\varepsilon = \int_T \int_{\Gamma_1} \sigma(\theta(x, t)^4 - \theta_{\text{amb}}^4) \psi(x, t) dt dx + \int_T \int_{\Gamma_2} \sigma(\theta(x, t)^4 - \theta_{\text{hot}}^4) \psi(x, t) dt dx$$

- the cost function gradient for $z = h(\theta)$ is:

$$\nabla J_h = \int_T \int_{\Gamma_1} (\theta(x, t) - \theta_{\text{amb}}) \psi(x, t) dt dx$$

Then, the minimization algorithm reads as follows:

- (1) Initialization of the direct problem with f^0 .
- (2) Resolution of the direct problem in order to determine the cost function $J(\theta, f^n)$.
The if the stopping condition (usually linked to a desired minimum threshold) is satisfied, the convergence is assumed to be achieved, else a further iteration is implemented.
- (3) Resolution of the adjoin problem in order to determine the cost function gradient $\nabla J(\theta, f^n)$.
- (4) Determination of the descent direction d^n : $d^n = \nabla J^n(\theta, f^n) + \beta_n d^{n-1}$ where $\beta_n = \|\nabla J(\theta, f^n)\| / \|\nabla J(\theta, f^{n-1})\|$
- (5) Resolution of the sensitivity problem in order to estimate the descent depth γ_n .
- (6) Estimation of the unknown function at iteration $n + 1$ according to the formula: $f^{n+1} = f^n + \gamma_n d^n$ and return to step 2 (with $n = n + 1$).

For the stopping condition, the desired minimum threshold is estimated from the noise distribution statistical properties at each sensor and for any step time, [17] and [22].

7.2. Emissivity identification

For temperature observations required for emissivity identification, vacuum conditions are imposed in the PACVD reactor (about $\approx 10^{-6}$ torr) in order to neglect convective phenomena. The cost function evolution versus minimization algorithm iteration number is presented in figure 15.

Even if $J(f)$ is still decreasing, it is important to stop the minimization algorithm while the desired threshold is reached in order to avoid oscillations of the identified function. For example, in figure 16, solution at iteration 20 seems to be better than solution at iteration 36.

Emissivity identified at iteration 20 can be considered as a good estimation since the relative error between calculated and measured temperatures is less than 2% (figures 17 and 18).

For measured temperature close to the ambient temperature, the emissivity coefficient is quite difficult to estimate since sensitivity function is too small. For high temperature, the emissivity coefficient is not correctly estimated because the adjoin function is fixed equal to zero at the end of the time interval. Considering the identified

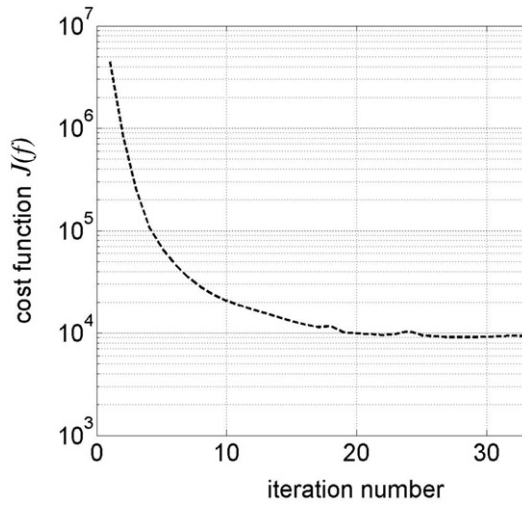


Figure 15. Quadratic criterion vs. iteration number for emissivity identification.

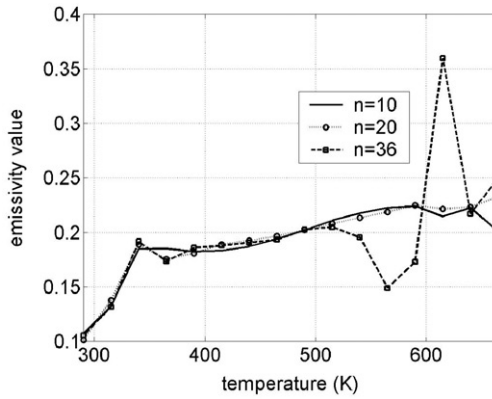


Figure 16. Identified temperature dependent emissivity.

value for the emissivity, the estimation of the convective exchange coefficient can be investigated.

7.3. Convective exchange coefficient identification

The identification of the convective exchange coefficient is performed according to further experimental measurements. The convergence of the cost function is achieved after the fourth iteration (figure 19), and temperature-dependent convective heat exchange coefficients are shown in figure 20 for several iterations.

Convective heat exchange coefficient identified at iteration 4 can be considered as a good estimation since the relative error between calculated and measured temperatures is less than 2% (figures 21 and 22) even if for high temperature, estimation is not correct (since the adjoint function is fixed equal to zero at the end of the time interval).

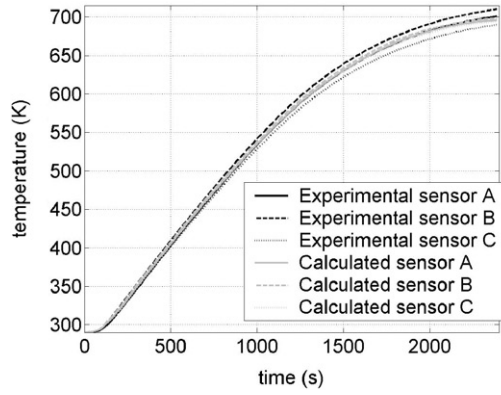


Figure 17. Measured and calculated temperatures at iteration 20.

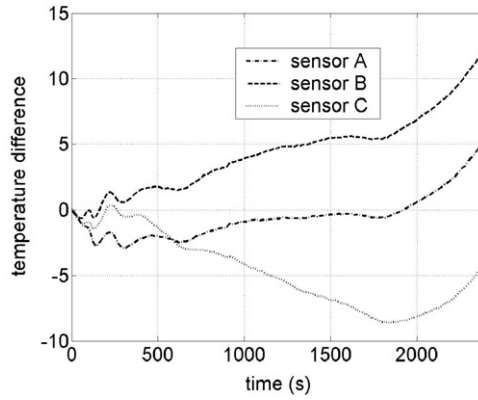


Figure 18. Residues between measured and calculated temperature at iteration 20.

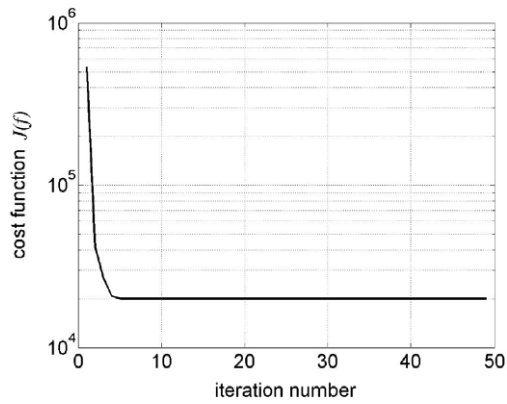


Figure 19. Quadratic criterion vs. iteration number for convective exchange coefficient identification.

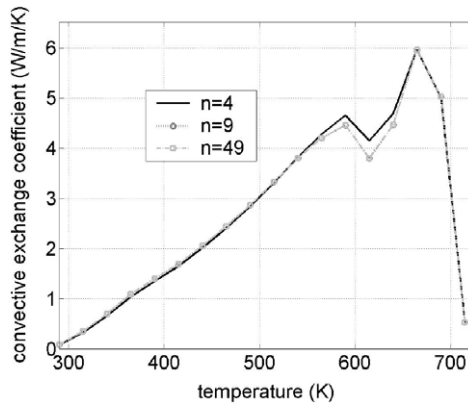


Figure 20. Identified convective heat exchange coefficient.

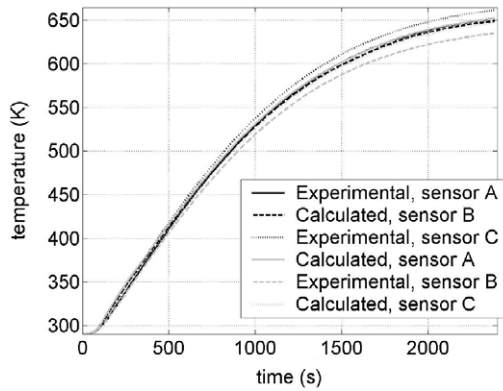


Figure 21. Measured and calculated temperatures at iteration 4.

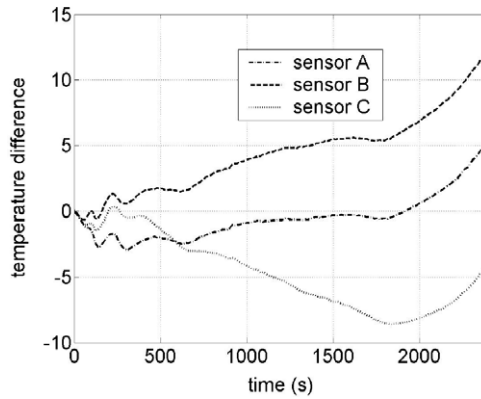


Figure 22. Residues between measured and calculated temperature at iteration 4.

8. Conclusions

In this communication, a methodology for finding the factors of influence in a thermal model has been exposed and carried out in an experimental situation. Based upon the DOE method, this screening approach has been proposed in order to determine which thermophysical factors of a mathematical model (describing the heat transfer in a reactor) are not known with a sufficient accuracy and do not lead to valid predictive simulation results. A PACVD process is investigated and thermal evolution of the material during the coating is described by a set of nonlinear partial differential equations. The numerical design of experiment method is implemented and it is shown that two factors among seven have to be carefully estimated: the convective exchange coefficient which is influenceable on the steady state of the substrate and the emissivity coefficient which is influenceable on the system dynamics. Then a more conventional approach is considered in order to determine the sensitivity functions. Two sensitivity problems derived from the direct problem are solved and lead to optimal measurements strategies for inverse problem resolution. Experimental results are exposed and a conjugate gradient algorithm is implemented in order to minimize a quadratic criterion (difference between the simulated and the measured state) and to achieve the unknown parameters identification. For further investigations, based on the efficient predictive tool validated in this communication, optimization of the PACVD reactor can be performed in order to control the thermal state of the substrate surface.

References

- [1] Satelli, A., Tarantola, S., Campolongo, F. and Ratto, M., 2004, *Sensitivity Analysis in Practice: A Guide to Assessing Scientific Models* (New York: Wiley).
- [2] Myers, R.H. and Montgomery, D.C., 2002, *Response Surface Methodology: Process and Product Optimisation Using Designed Experiments*, 2nd Edn (New York: Wiley).
- [3] Drain, D., 1997, *Handbook of Experimental Methods for Process Improvement* (New York: Chapman and Hall).
- [4] Schimmerling, P., 1987, Fiabilité prévisionnelle en fatigue et plans d'expériences numériques. *Revue de la SIA - Société des Ingénieurs en Automobile*, **2**, 88–93.
- [5] Schimmerling, P., 1989, Comment accroître la durée de vie des soufflets de transmission avec les plans d'expériences numériques et la méthodologie Taguchi. *Revue de la SIA-Société des Ingénieurs en Automobile*, **1**, 67–73.
- [6] Frenklach, M., Wang, H. and Rabinowitz, M.J., 1992, Optimization and analysis of large chemical kinetic mechanisms using the solution mapping method – Combustion of methane. *Progression Energy Combustion Science*, **18**, 47–73.
- [7] Bettonvil, B. and Kleijnen, J.P.C., 1996, Searching for important factors in simulation models with many factors: sequential bifurcation. *European Journal of Operational Research*, **96**, 180–194.
- [8] Kleijnen, J.P.C. and Sargent, R.G., 2000, A methodology for fitting and validating metamodels in simulation. *European Journal of Operational Research*, **120**, 14–29.
- [9] Houston, D.X., Ferreira, S., Collofello, J.S., Montgomery, D.C., Mackulak, G.T. and Shunk, D.L., 2001, Behavioral characterization: Finding and using the influential factors in a software process simulation models. *The Journal of Systems and Software*, **59**, 259–270.
- [10] Bacour, C., Jacquemoud, S., Tourbier, Y., Dechambre, M. and Frangi, J.P., 2002, Design and analysis of numerical experiments to compare four canopy reflectance models. *Remote Sensing of Environment*, **79**, 72–83.
- [11] Russel, W.C., 1995, Experimental design approach to development of a CVD ZrN coating. *Journal de Physique IV*, **5**, C5-127–C5-134.
- [12] De Legé, L.J. and Hendriks, M., 1991, Characterization and optimization of the LPCVD silicon oxynitride process, using the design of experiment method. *Journal de Physique IV*, **1**, C2-47–C2-54.
- [13] Boher, C., Ducarroir, M., Grégoire, T. and Scordo, S., 1998, Comportement en frottement sec de dépôts SiC_x(H) (1,5 < x < 3) élaborés par PACVD micro-onde sur acier. *Les Annales de Chimie, Sciences des Matériaux*, **23**, 879–890.

- [14] Grill, A., 1993, *Cold Plasma in Materials Fabrication* (New York: IEEE Press).
- [15] Chapman, B., 1980, *Glow Discharge Processes* (New York: Wiley Interscience).
- [16] Thomas, L., Maillé, L., Badie, J.M. and Ducarroir, M., 2001, Microwave plasma chemical vapor deposition of tetramethylsilane: Correlations between optical emission spectroscopy and film characteristics. *Surface and Coatings Technology*, **142–144**, 314–320.
- [17] Alifanov, O.M., 1994, *Inverse Heat Transfer Problems* (Berlin: Springer-Verlag).
- [18] Box, G.E.P. and Draper, N.R., 1987, *Empirical Model-Building and Response Surfaces, Series in Probability and Mathematical Statistics* (New York: Wiley).
- [19] Montgomery, D.C., 1997, *Design and Analysis of Experiments* (New York: Wiley).
- [20] Box, G.E.P., Hunter, W.G. and Hunter, J.S., 1978, *Statistics for experimenters – An Introduction to Design, Data Analysis and Model Building* (New York: Wiley).
- [21] Abou Khachfe, R. and Jarny, Y., 2001, Determination of heat sources and heat transfer coefficient for two dimensional heat flow – numerical and experimental study. *International Journal of Heat and Mass Transfer*, **44**, 1309–1322.
- [22] Alifanov, O.M., Artyukhin, E.A. and Rumyantsev, S.V., 1995, *Extreme Methods for Solving Ill-Posed Problems with Applications to Inverse Heat Transfer Problems* (New York: Begell house Inc).